Available online at www.sciencedirect.com

ScienceDirect

Ceramics International 40 (2014) 4767–4775

CERAMICS INTERNATIONAL

www.elsevier.com/locate/ceramint

Characterization and photocatalytic properties of hexagonal and monoclinic WO_3 prepared via microwave-assisted hydrothermal synthesis

Diana B. Hernandez-Uresti[a], D. Sánchez-Martínez[b,*], A. Martínez-de la Cruz[a], S. Sepúlveda-Guzmán[a], Leticia M. Torres-Martínez[b]

[a]*Universidad Autónoma de Nuevo León, Facultad de Ingeniería Mecánica y Eléctrica, Cd. Universitaria, C.P. 66451, San Nicolás de los Garza, N.L., Mexico*
[b]*Universidad Autónoma de Nuevo León, Facultad de Ingeniería Civil, Departamento de Ecomateriales y Energía, Cd. Universitaria, C.P. 66451, San Nicolás de los Garza, N.L., Mexico*

Received 29 July 2013; received in revised form 6 September 2013; accepted 7 September 2013
Available online 16 September 2013

Abstract

WO_3 nanoparticles with hexagonal and monoclinic structures were synthesized via a microwave-assisted hydrothermal process without the use of any additives in which the microwave hydrothermal reaction time was 30 or 60 min and was followed by different thermal treatments. The formation at different temperatures of hexagonal (h-WO_3) and monoclinic (m-WO_3) crystal structures of WO_3 was confirmed by X-ray powder diffraction (XRD). The characterization of WO_3 samples was complemented with scanning electron microscopy (SEM) images, which revealed a natural tendency of the oxides to form particles with ovoid shapes. The particle size of the prepared WO_3 samples was between 20 and 100 nm depending on the heat-treatment temperatures. The surface areas of the WO_3 samples, as determined by the BET method, ranged from 2 to 113 $m^2 g^{-1}$ depending on their temperature of synthesis. The highest obtained specific surface area was nearly 37 times greater than that observed for commercial WO_3. The photocatalytic activity of WO_3 was evaluated with respect to the degradation reactions of rhodamine B (rhB), indigo carmine (IC) and tetracycline hydrochloride (TC) under UV–vis irradiation. The highest activity was observed in the sample obtained by thermal treatment at 700 °C and with a microwave hydrothermal reaction time of 30 min. The degree of mineralization of the organic dyes by WO_3 was determined by the total organic carbon analysis (TOC) and was found to reach percentages of 95% for rhB, 65% for IC and 65% for TC after 96 h of irradiation.

Keywords: Hexagonal WO_3; Monoclinic WO_3; Microwave-assisted hydrothermal synthesis; Photocatalysis

1. Introduction

Throughout the last decade, the study of transition-metal oxides has become important due to their potential applications, which include nanoelectronics [1], gas sensors [2,3], optical devices [4], electrochromic devices [5,6], catalysts [7–9] and photocatalysts in a large variety of chemical reactions [10–15]. In particular, tungsten oxide (WO_3) is of great interest in the scientific community because it is an inexpensive material with high stability in aqueous solutions under acidic conditions, it does not undergo a photocorrosion process and it exhibits polymorphism.

Among the polymorphs of WO_3, the phases that have attracted the most attention are the hexagonal phase (h-WO_3) and the monoclinic phase (m-WO_3). The hexagonal phase has drawn special interest in gas-sensor applications, among others, because of its open-tunnel structure and rich intercalation chemistry. The monoclinic phase is an attractive candidate for photocatalytic applications under solar irradiation because it exhibits the proper band-gap energy for the adsorption of visible light [16–18]. For these reasons, the synthesis of WO_3 has attracted special attention, and researchers have attempted to prepare it through various methods, including decomposition [19], acid precipitation [20], sol–gel [21], electrospinning [22] and hydrothermal treatment routes [23,24], among others. With all of these methods, the monoclinic phase (m-WO_3) is commonly obtained due to its thermodynamic stability at room temperature; the hexagonal phase (h-WO_3) is commonly

*Corresponding author. Tel.: +52 81 1442 4400; fax: +52 81 1442 4443.
E-mail address: dansanm@gmail.com (D. Sánchez-Martínez).

0272-8842/$ - see front matter © 2013 Elsevier Ltd and Techna Group S.r.l. All rights reserved.
http://dx.doi.org/10.1016/j.ceramint.2013.09.022

Table 1
Research reported in the literature on the preparation of WO_3 via microwave-assisted hydrothermal processes.

Sample	Synthesis method	Used additive	Phase obtained	Experimental conditions	Reference
$WO_3 \cdot 2H_2O$ nanospheres	Microwave hydrothermal process	Tartaric acid	$WO_3 \cdot 2H_2O$	Mixture was transferred into a 300 mL Teflon container and then treated in a domestic microwave for 20 min	[26]
WO_3 nanoparticles	Solvothermal under microwave	Benzyl alcohol	Cubic	The solution was introduced in a Teflon reactor at 210 °C. Then the solution was irradiated by microwave. Finally the solution was calcined between 300 and 500 °C	[27]
WO_3 nanoplates	Microwave hydrothermal method	Citric acid	Mixed phases and monoclinic	The solution was transferred to the lab-made autoclave and processed at 270 W via microwave radiation for 180 min	[28]
WO_3 nanoparticles	Microwave-assisted hydrothermal	Without additive	Hexagonal and monoclinic	The solution was transferred to a microwave-assisted hydrothermal reactor at 180 °C, 200 W fo 30 and 60 min	This work

obtained via hydrothermal methods because of its metastability.

Among these methods, the synthesis via hydrothermal process is the more commonly used approach for the synthesis of h-WO_3 and m-WO_3 phases [23,24]. However, this method usually requires prolonged reaction times that range from several hours to several days for the formation of the oxide [1,25]. Therefore, few studies in the existing literature have been focused on the preparation of h-WO_3 and m-WO_3 nanoparticles via a microwave-assisted hydrothermal method, as is shown in Table 1. Most of the methods reported in the literature on the preparation of WO_3 powders via the microwave-assisted hydrothermal method have involved the use of one or more additives (see Table 1).

In this work, h-WO_3 and m-WO_3 nanoparticles were successfully prepared via a microwave-assisted hydrothermal method without the use of any additives. The samples were characterized, and their photocatalytic properties were evaluated in the degradation of two organic dyes and an antibiotic: rhodamine B (rhB, CAS 81-88-9), indigo carmine (IC, CAS 860-22-0) and tetracycline hydrochloride (TC, CAS 64-75-5) under UV–vis irradiation.

2. Experimental

2.1. Synthesis of hexagonal and monoclinic WO_3

WO_3 nanoparticles with hexagonal and monoclinic structures were obtained via microwave-assisted hydrothermal treatments of aqueous solutions. For this purpose, 5.50 g of ammonium tungstate hydrate ($H_{42}N_{10}O_{42}W_{12} \cdot xH_2O$, 99% purity, Sigma-Aldrich) was dissolved under continuous stirring in 50 mL of nitric acid solution (10% v/v, HNO_3). Afterwards, the pH of the solution was adjusted under stirring to approximately 3 by the dropwise addition of ammonium hydroxide solution (NH_4OH, 30% Reagents DUKSAN), and the stirring was maintained until a homogeneous solution was formed. Then, the aqueous solution was transferred to a microwave-assisted hydrothermal reactor, which was heated at 180 °C under a magnetron power of 200 W applied for 30 or 60 min. The powder obtained from this step was washed several times with distilled water and ethanol to neutralize the pH of the solution and was dried in air at 70 °C for 24 h. The powders were thermally treated from room temperature to the specific temperature (250, 500 or 700 °C) under air atmosphere with a heating rate of 10 °C min^{-1}.

2.2. Characterizations of WO_3 samples

Structural characterization of h-WO_3 and m-WO_3 was performed by X-ray powder diffraction analysis using a Bruker D2 PHASER diffractometer equipped with a CuKα radiation source ($\lambda = 1.5418$ Å). X-ray diffraction data of samples were collected in the 2θ range of 10–70° with a step size of 0.02° and a scan rate of 0.2 s^{-1}. The morphologies and particle sizes of the samples were investigated by scanning electron microscopy using a FEI Nova 200 NanoSEM microscope.

The band-gap energy (E_g) was determined by means of UV–vis diffuse-reflectance absorption spectroscopy of the WO_3 samples, which was collected on a PerkinElmer Lambda 35 UV–vis spectrophotometer equipped with an integrating sphere. The BET surface areas and mean pore diameters of the WO_3 samples were determined by adsorption–desorption N_2 isotherms using a BELSORP Mini-II surface-area and pore-size analyzer. The isotherms were evaluated at −196 °C after the samples were degassed by a heat treatment at 150 °C for 24 h.

2.3. Photocatalytic experiments

The photocatalytic activities of WO_3 samples toward the degradation of rhodamine B (rhB), indigo carmine (IC) and tetracycline hydrochloride (TC) in aqueous solution were evaluated. Fig. 1 shows the molecular structures of the two dyes and the antibiotic used to evaluate the activity of the WO_3 samples. The reactor used was a homemade device that consisted of a borosilicate glass beaker embedded in a water jacket to maintain the reaction temperature at 25 ± 1 °C. A 6000-K Xe lamp with a luminous flux of 90,500 lx was used as a UV–vis radiation source.

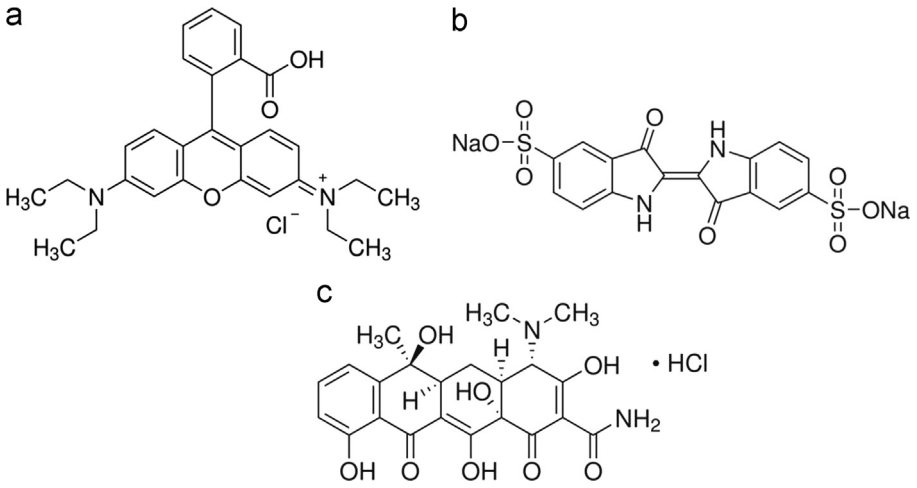

Fig. 1. Chemical structures of a) rhodamine B, b) indigo carmine and c) tetracycline hydrochloride.

Experiments were conducted in a glass beaker, where 200 mL of the solution to be degraded (dye or antibiotic) that contained 200 mg of WO_3 powder was placed in an ultrasonic bath for 2 min to eliminate aggregates. The solution was then transferred to the photochemical reactor. By considering the molar extinction coefficients of dyes, we determined their initial concentrations to be 5 mg L^{-1} for rhB and 30 mg L^{-1} for IC and for the TC a concentration of 20 mg L^{-1} was used. The solution was kept in dark for 1 h to ensure that adsorption–desorption equilibrium of the organic compound on the catalyst was reached. After this time, the light source was turned on. During the reaction, samples were collected from the reactor at different time intervals and were subsequently analyzed using UV–vis spectrophotometry according to the procedure established elsewhere [29].

The degree of mineralization was monitored through analysis of the total organic carbon (TOC) content in the irradiated solutions at different time intervals using a SHIMADZU TOC-VSCH analyzer. A typical experiment consisted of 200 mL of the solution to be degraded (50 mg L^{-1} for rhB, 100 mg L^{-1} for IC and 50 mg L^{-1} for TC) that contained 200 mg of the photocatalyst.

3. Results and discussion

3.1. Structural characterization

The obtained powders (30 and 60 min) were decomposed by heat treatments at 250, 500 or 700 °C. The solids obtained were greenish, and the calcined samples were characterized by a greenish-yellow tint. The formation of the hexagonal and monoclinic WO_3 phases (hereafter identified as h-W30, h-W30-250, m-W30-500, m-W30-700, h-W60, h-W60-250, m-W60-500 and m-W60-700) was followed by X-ray powder diffraction. Fig. 2 shows X-ray diffraction patterns of samples synthesized at 30 or 60 min and under heat treatments at 250, 500 or 700 °C. We observed that, in the cases of the samples synthesized at both reactions times, the products prepared without a heat treatment (h-W30 and h-W60) and those heated

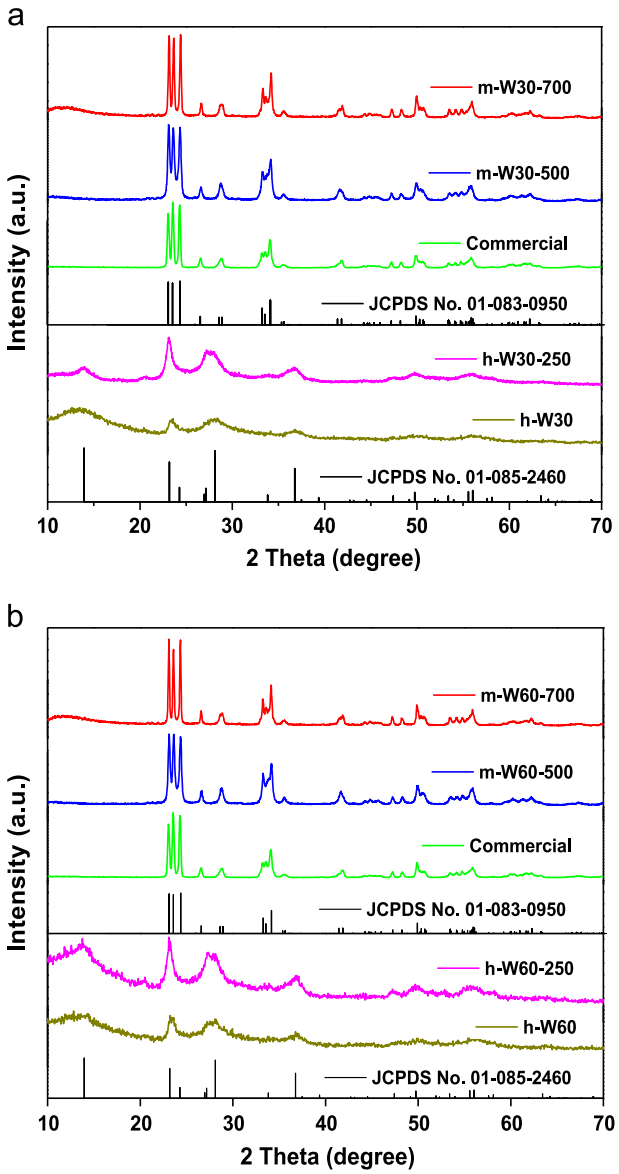

Fig. 2. X-ray powder diffraction patterns of WO_3 samples synthesized with a) 30 min and b) 60 min of microwave-hydrothermal reaction followed by heat treatments at 250, 500 or 700 °C.

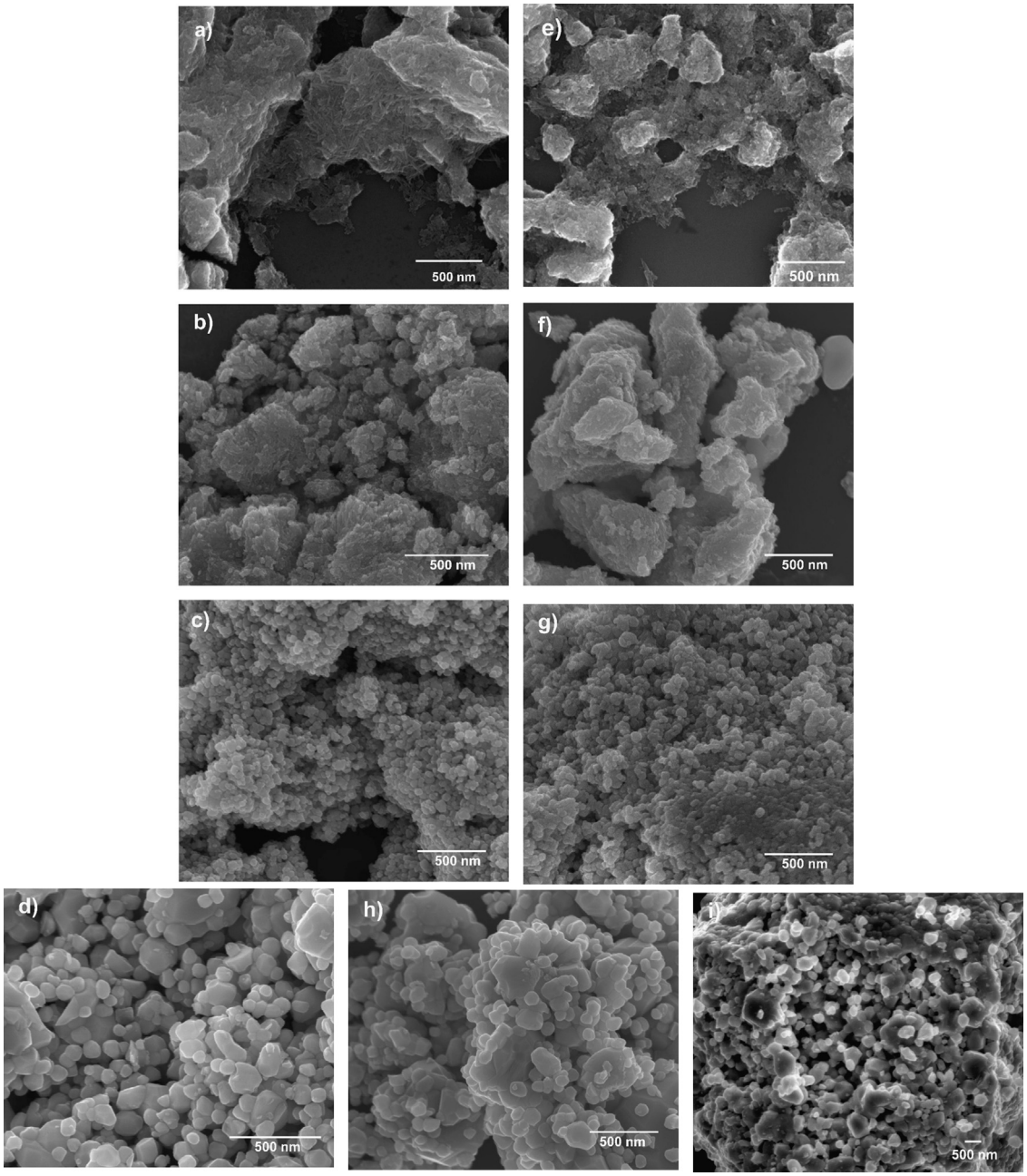

Fig. 3. SEM images of WO_3 nanoparticles synthesized by a microwave-assisted hydrothermal method with 30 min of microwave-hydrothermal reaction a) without heat treatment, with heat treatment at b) 250 °C, c) 500 °C, or d) 700 °C and with 60 min of microwave hydrothermal reaction e) without heat treatment and with heat treatment at f) 250 °C, g) 500 °C and h) 700 °C; image i) represents a commercial oxide.

at 250 °C (h-W30-250 and h-W60-250) crystallized in the hexagonal polymorph of WO_3 (h-WO_3) according to JCPDS card No. 01-085-2460. In these samples, the diffraction peaks located at $2\theta = 13.9^\circ$, 23.2°, 28.1° and 36.7° were associated with the main diffraction lines of h-WO_3. When the obtained powders were calcined at 500 or 700 °C, the powders that reacted for both 30 and 60 min underwent transitions in crystallinity from h-WO_3 to m-WO_3 according to JCPDS card No. 01-083-0950. In all cases, only diffraction lines associated with the WO_3 monoclinic structure were observed. In particular, the intensities of the diffraction lines in the XRD patterns of the samples prepared at the higher temperature (700 °C) increased and were better defined. This fact is associated with a significant increase in the crystallinity of the samples at high temperatures.

3.2. Morphological characterization

The morphologies and particle sizes of the WO_3 samples were analyzed by SEM. Fig. 3 shows some SEM micrographs of h-WO_3 and m-WO_3 oxides obtained via the microwave-assisted hydrothermal method under different experimental conditions. Agglomerates with sizes of approximately 500 nm were observed in the micrographs of powders prepared with

Table 2
Physical properties of WO_3 samples.

Sample	E_g (eV)	BET surface area ($m^2\,g^{-1}$)	Mean pore diameter (nm)
Commercial	2.62	3.3	40.17
h-W30	2.50	113.5	3.09
h-W30-250	2.76	74.2	4.77
m-W30-500	2.69	12.7	26.36
m-W30-700	2.67	4.5	64.35
h-W60	2.57	111.8	2.75
h-W60-250	2.76	68.9	3.66
m-W60-500	2.70	12.5	24.81
m-W60-700	2.69	1.8	56.53

and without heat treatment at 250 °C; agglomerates were formed principally by smaller particles with diameters between 20 and 50 nm, as shown in Fig. 3a, b (h-W30, h-W30-250) and in Fig. 3e, f (h-W60, h-W60-250). When the temperature of synthesis was increased to 500 °C, particles of m-W30-500 (Fig. 3c) and m-W60-500 (Fig. 3g) were characterized by an ovoid morphology and a tendency to form agglomerates with particle sizes of approximately 50 nm. For the samples prepared at 700 °C, m-W30-700 (Fig. 3d) and m-W60-700 (Fig. 3h), the SEM images show ovoid particles with smooth surfaces and particles sizes of approximately 100 nm. In this case, the average particle size was increased by the elimination of grain boundaries via the sintering process.

Our main conclusion from these results is that the morphology of WO_3 samples was not affected by the microwave hydrothermal reaction time (30 and 60 min). The formation of ovoid particles appears to be a natural tendency of the monoclinic WO_3 system, as was also observed when commercial WO_3 was analyzed, as shown in Fig. 3i.

3.3. Band-gap energy and BET surface area analysis

The optical properties of WO_3 samples were analyzed by UV–vis diffuse reflectance spectroscopy. Table 2 shows the band-gap energy (E_g) values of the synthesized samples. The E_g values found are within the range reported in the literature (i.e., 2.5–2.8 eV [16–18]) and are similar to the E_g value of commercial WO_3.

The surface areas and mean pore diameters of WO_3 samples measured by the BET method are also included in Table 2. As expected, the surface areas of the samples decreased as the synthesis temperature was increased due to the growth of the WO_3 particles, and mean pore diameter was directly proportional to the temperature. For these reasons, the highest specific surface area was achieved with the powders obtained directly via the microwave hydrothermal reaction (without heat treatment) at both synthesis times (113.5 $m^2\,g^{-1}$ for h-W30 and 111.8 $m^2\,g^{-1}$ for h-W60). These values are nearly 37 times greater than that observed for the commercial WO_3. Fig. 4 shows the adsorption–desorption isotherms of WO_3 samples. In general, two types of profiles were observed in the samples analyzed. In the first instance, materials with the hexagonal crystalline structure (h-W30, h-W30-250, h-W60 and h-W60-250) showed adsorption–desorption isotherms typical of mesoporous materials (i.e., type IV isotherms according to the classification previously established for adsorption–desorption isotherms [30]), as shown in Fig. 4a, b, e and f, respectively. However, the samples with the monoclinic crystalline structure, i.e., m-W30-500, m-W30-700, m-W60-500 and m-W60-700, exhibited behaviors typical of macroporous materials (i.e., type II isotherms), as shown in Fig. 4c–h.

As the main conclusion from these results, the WO_3 samples with the highest specific surface area values and hexagonal crystalline structures are potential candidates for gas-sensor applications according to reports in the literature, where materials with a large surface area showed a high sensitivity to the detection of toxic gases [31].

3.4. Photocatalytic activity of WO_3 samples

The photocatalytic activity of WO_3 samples was evaluated in the degradation reactions of rhB, IC and TC molecules in water under a 6000-K Xe lamp as a radiation source. Fig. 5 shows the degradation of rhodamine B (5 mg L^{-1}) with different synthesized WO_3 samples used as photocatalysts. After 240 min of exposure to lamp irradiation, all of the samples bleached the rhB solution to a large degree. All the samples exhibited better results than that of commercial WO_3. In particular, the m-W30-500 and m-W30-700 samples bleached nearly 100% of the rhB solution. Although the photocatalytic activities of the WO_3 samples were similar, the samples synthesized at higher temperatures (m-W30-700 and m-W60-700) showed slightly better bleaching performance compared to the samples synthesized at lower temperatures (m-W30-500 and m-W60-500).

These results indicate that the temperature at which the obtained powders were thermally treated played a role as important as that of the time of microwave hydrothermal reaction in determining the photocatalytic properties of the WO_3 samples. These results differ from the characterization results for the samples, where physical properties related to the morphology as well as optical and textural properties were not influenced by the time of microwave hydrothermal reaction. In contrast, significant differences were observed in these physical properties when the temperature of the thermal treatment was modified.

The surface area and degree of crystallinity of the photocatalyst can play a determinant role in the photocatalytic activity. Unfortunately, these factors work in opposite directions, i.e., samples with a higher surface area can be obtained at lower temperatures but with a low degree of crystallinity. The first case leads to a high concentration of defects on the crystalline structure of the oxide. These defects function as undesirable recombination points of electrons and holes formed during the excitation of the semiconductor oxides under irradiation. Although notable differences were observed in the surface-area values of samples prepared using the same reaction time (30 or 60 min), the surface area does not significantly influence the activity of the oxide. In this sense,

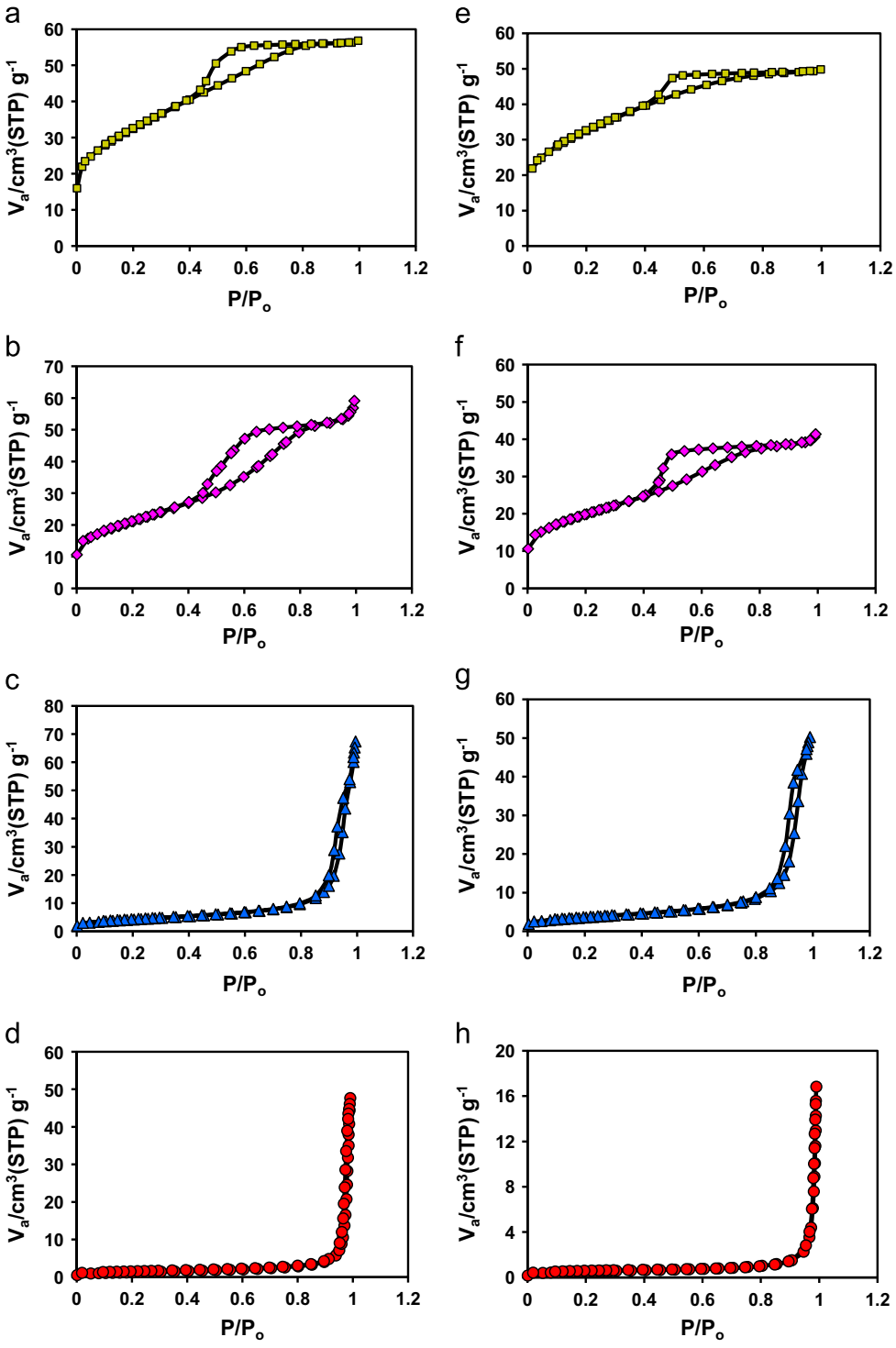

Fig. 4. N_2 adsorption–desorption isotherms of WO_3 samples prepared by microwave-assisted hydrothermal method with 30 min of microwave-hydrothermal reaction a) without heat treatment and with heat treatment at b) 250 °C, c) 500 °C or d) 700 °C and with 60 min of microwave hydrothermal reaction e) without heat treatment and with heat treatment at f) 250 °C, g) 500 °C or h) 700 °C.

the factor that governs the photocatalytic activity of the WO_3 nanoparticles is the degree of crystallinity of the photocatalyst. This behavior was observed in a previous work, where the activity of WO_3 samples was increased when the temperature of the thermal treatment to form the oxide was increased [14]. Because the hexagonal-structured samples (h-W30, h-W30-250, h-W60 and h-W60-250) showed strong adsorption of the rhB molecules at their surfaces, photocatalytic experiments were not performed with these materials.

Fig. 6 shows the evolution of concentration of IC (30 mg L^{-1}) in the course of its photocatalytic degradation by Xe lamp irradiation. The reaction rate of IC degradation was greater than that observed for rhB, as can be deduced from the time required for the WO_3 samples to bleach the IC solutions.

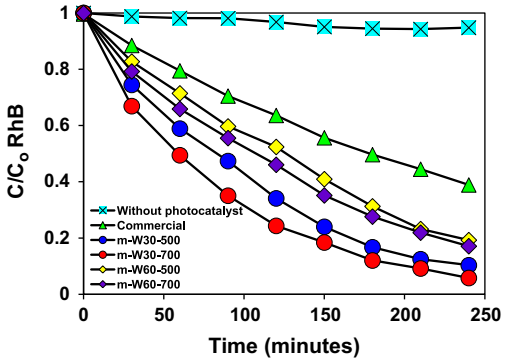

Fig. 5. Photocatalytic degradation of rhB (5 mg L^{-1}) under UV–vis irradiation; the photocatalyst was WO_3 synthesized under different experimental conditions.

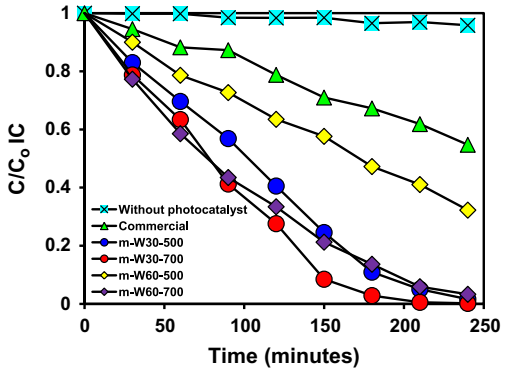

Fig. 6. Photocatalytic degradation of IC (30 mg L^{-1}) under UV–vis radiation; the photocatalyst was WO_3 synthesized under different experimental conditions.

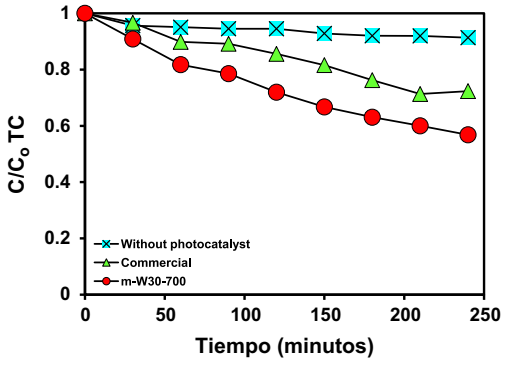

Fig. 7. Photocatalytic degradation of TC (20 mg L^{-1}) under UV–vis radiation; the photocatalyst was WO_3 synthesized under different experimental conditions.

Notably, the initial IC concentration used in these experiments was six times greater than that used in the rhB experiments because of their respective molar extinction coefficients. With the exception of m-W60-500, all of the samples bleached the IC solution to nearly 100% within 180 min. These experiments revealed that the degradation of rhB and IC is feasible when WO_3 is used as a photocatalyst.

Fig. 7 shows the evolution of the concentration of TC (20 mg L^{-1}) in the presence of m-W30-700 as a photocatalyst

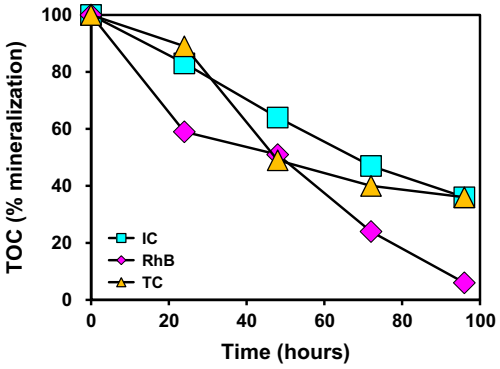

Fig. 8. Changes in the TOC during the mineralization of rhB, IC and TC.

in the course of its photocatalytic degradation under irradiation by a Xe lamp. In this test, only the WO_3 sample that exhibited the best photocatalytic activity toward the degradation of rhB and IC was used. After 240 min of irradiation, the m-W30-700 degraded almost 50% of the TC solution, which was better than the performance achieved with the commercial WO_3. Therefore, on the basis of these results, we can conclude that use of WO_3 as a photocatalyst is feasible not only in the degradation of organic dyes but also in the degradation of antibiotics, such as tetracycline, which can undergo a series of pathological changes and disrupt ecosystem equilibrium [32].

To determine if the mineralization of organic compounds by the WO_3 oxides is feasible, we performed analyses of the total organic carbon (TOC) during the course of the photocatalytic reaction for the degradation of rhB, IC and TC, as is shown in Fig. 8. For these experiments, we used the sample with the highest photocatalytic activity, m-W30-700, as a photocatalyst. To minimize the experimental error, the initial concentrations of rhB, IC and TC were modified to 50 mg L^{-1}, 100 mg L^{-1} and 50 mg L^{-1}, respectively. The degree of mineralization reached after 96 h under lamp irradiation was 95% for rhB, 65% for IC and 65% for TC. These results indicate that not only the chromophore group but also the aromatic rings in the rhB and IC molecules are attacked during the photocatalytic reaction. Similarly, these results indicate that the destruction of TC is possible.

Unlike the previous works [13,14], this work involved the successful preparation of WO_3 nanoparticles via a microwave-assisted hydrothermal method without the use of any additives in which the time of the microwave hydrothermal reaction (30 or 60 min) was varied and the effect of the temperature during different thermal treatments was studied. The results obtained from the characterization of the samples indicated that physical properties such as the morphology as well as optical and textural properties were not influenced by the microwave hydrothermal reaction time. In contrast, significant differences were observed in these physical properties when the temperature of the thermal treatments was modified. However, the microwave hydrothermal reaction time and the temperatures of the thermal treatments played an important role in the photocatalytic properties of the WO_3 samples.

Therefore, using this synthesis method, we prepared WO_3 samples with interesting and attractive physicochemical

properties, which we observed via our characterization of their structural, morphological, optical and textural properties. In addition, the prepared oxides exhibited good photocatalytic properties with respect to the photodegradation of two organic dyes (rhB and IC) and an antibiotic (TC).

4. Conclusions

WO_3 nanoparticles with hexagonal and monoclinic structures were successfully synthesized via a microwave-assisted hydrothermal method without the use of any additives in which the microwave hydrothermal reaction time was varied (30 or 60 min) and different thermal treatments were used. Using this route, we prepared hexagonal-structured WO_3 at lower temperatures ($\leqslant$250 °C) and the monoclinic polymorph at higher temperatures ($\geqslant$500 °C); i.e., the WO_3 undergoes a crystallinity transition from h-WO_3 to m-WO_3 due to the effect of the temperature increase in materials prepared at both reaction times. For all the prepared samples, the morphology of the WO_3 particles was ovoid. The particle sizes of obtained WO_3 samples were between 20 and 100 nm depending on the heat-treatment temperature. The WO_3 samples with hexagonal structures exhibited the greatest specific surface area. Samples of the synthesized WO_3, when used as photocatalysts, exhibited greater photocatalytic activity than the commercial WO_3 toward the degradation of rhB, IC and TC in aqueous solutions under irradiation by a Xe lamp. Hexagonal-structured samples of WO_3 exhibited strong adsorption; for this reason, they were not used in the photocatalytic experiments. Monoclinic-structured WO_3 samples exhibited the highest activity when they had been thermally treated at 700 °C and had been prepared at a microwave-hydrothermal reaction time of 30 min, probably due to optimized values of synthesis temperature, reaction time and crystallinity. After 96 h under lamp irradiation, the mineralization of the organic dyes and the antibiotic was complete: 95% for rhB, 65% for IC and 65% for TC. These results corroborate the potential of WO_3 as a photocatalyst in the removal of organic dyes and antibiotics.

Acknowledgments

We wish to thank the Universidad Autónoma de Nuevo León (UANL) for its invaluable support through Project PAICYT 2011–2012; CONACYT, for support of Projects "Repatriación clave 166008", CB-2008 Clave 98740, FON. INST./75/2012 "FOTOSÍNTESIS ARTIFICIAL" and CNPq MÉXICO-BRASIL 2012 Clave 174247; and SEP, for support of Project PIFI 2011-2012 Apoyo al CA-UANL-244.

References

[1] R. Huirache-Acuña, F. Paraguay-Delgado, M.A. Albiter, J. Lara-Romero, R. Martínez-Sánchez, Synthesis and characterization of WO_3 nanostructures prepared by an aged-hydrothermal method, Materials Characterization 60 (2009) 932–937.

[2] S. Ashraf, C.S. Blackman, R.G. Palgrave, I.P. Parkin, Aerosol-assisted chemical vapour deposition of WO_3 thin films using polyoxometallate precursors and their gas sensing properties, Journal of Materials Chemistry 17 (2007) 1063–1070.

[3] E.H. Espinosa, R. Ionescu, E. Llobet, A. Felten, C. Bittencourt, E. Sotter, Z. Topalian, P. Heszler, C.G. Granqvist, J.J. Pireaux, X. Correig, Highly selective NO_2 gas sensors made of MWCNTs and WO_3 hybrid layers, Journal of the Electrochemical Society 154 (2007) J141–J149.

[4] A.A. Dakhel, Investigations on Sn-doped Ni oxide thin films and their use as optical sensor devices, Journal of Non-Crystalline Solids 358 (2012) 285–289.

[5] J. Zhang, X.L. Wang, X.H. Xia, C.D. Gu, J.P. Tu, Electrochromic behavior of WO_3 nanotree films prepared by hydrothermal oxidation, Solar Energy Materials and Solar Cells 95 (2011) 2107–2112.

[6] K.A. Gesheva, T.M. Ivanova, G. Bodurov, Transition metal oxide films: technology and Smart Windows electrochromic device performance, Progress in Organic Coatings 74 (2012) 635–639.

[7] H. Einaga, A. Ogata, Benzene oxidation with ozone over supported manganese oxide catalysts: effect of catalyst support and reaction conditions, Journal of Hazardous Materials 164 (2009) 1236–1241.

[8] H. Zou, S. Chen, Z. Liu, W. Lin, Selective CO oxidation over CuO–CeO_2 catalysts doped with transition metal oxides, Powder Technology 207 (2011) 238–244.

[9] K. Karásková, L. Obalová, K. Jirátová, F. Kovanda, Effect of promoters in Co–Mn–Al mixed oxide catalyst on N_2O decomposition, Chemical Engineering Journal 160 (2010) 480–487.

[10] F. Xu, D. Guo, H. Han, H. Wang, Z. Gao, D. Wu, K. Jiang, Room-temperature synthesis of pompon-like ZnO hierarchical structures and their enhanced photocatalytic properties, Research on Chemical Intermediates 38 (2012) 1579–1589.

[11] H. Cheng, Y. Huang, C. Lee, Decolorization of reactive dye using a photo-ferrioxalate system with brick grain-supported iron oxide, Journal of Hazardous Materials 188 (2011) 357–362.

[12] S. Sitthisang, S. Komarneni, J. Tantirungrotechai, Y.D. Noh, H. Li, S. Yin, T. Sato, H. Katsuki, Microwave-hydrothermal synthesis of extremely high specific surface area anatase for decomposing NO_x, Ceramics International 38 (2012) 6099–6105.

[13] D. Sánchez-Martínez, A. Martínez-de la Cruz, E. López-Cuéllar, Photocatalytic properties of WO_3 nanoparticles obtained by precipitation in presence of urea as complexing agent, Applied Catalysis A: General 398 (2011) 179–186.

[14] D. Sánchez-Martínez, A. Martínez-de la Cruz, E. López-Cuéllar, Synthesis of WO_3 nanoparticles citric acid-assisted precipitation and evaluation of their photocatalytic properties, Materials Research Bulletin 48 (2013) 691–697.

[15] Z. Zhu, D. Yang, H. Liu, Microwave-assisted hydrothermal synthesis of ZnO rod-assembled microspheres and their photocatalytic performances, Advanced Powder Technology 22 (2011) 493–497.

[16] G.R. Bamwenda, H. Arakawa, The visible light induced photocatalytic activity of tungsten trioxide powders, Applied Catalysis A: General 210 (2001) 181–191.

[17] X.F. Cheng, W.H. Leng, D.P. Liu, J.Q. Zhang, C.N. Cao, Enhanced photoelectrocatalytic performance of Zn-doped WO_3 photocatalysts for nitrite ions degradation under visible light, Chemosphere 68 (2007) 1976–1984.

[18] S.J. Hong, H. Jun, P.H. Borse, J.S. Lee, Size effects of WO_3 nanocrystals for photooxidation of water in particulate suspension and photoelectrochemical film systems, International Journal of Hydrogen Energy 34 (2009) 3234–3242.

[19] H. Yan, X. Zhang, S. Zhou, X. Xie, Y. Luo, Y. Yu, Synthesis of WO_3 nanoparticles for photocatalytic O_2 evolution by thermal decomposition of ammonium tungstate loading on g-C_3N_4, Journal of Alloys and Compounds 509 (2011) L232–L235.

[20] S. Supothina, P. Seeharaj, S. Yoriya, M. Sriyudthsak, Synthesis of tungsten oxide nanoparticles by acid precipitation method, Ceramics International 33 (2007) 931–936.

[21] M. Acosta Díaz, C. Vales Pinzón, I. Riech Méndez, WO_3 thin films by sol–gel: structural and morphological properties, Engineering 13 (3) (2009) 29–38.

[22] X. Lu, X. Liu, W. Zhang, C. Wang, Y. Wei, Large-scale synthesis of tungsten oxide nanofibers by electrospinning, Journal of Colloid and Interface Science 298 (2006) 996–999.

[23] J.H. Ha, P. Muralidharan, D.K. Kim, Hydrothermal synthesis and characterization of self-assembled h-WO_3 nanowires/nanorods using EDTA salts, Journal of Alloys and Compounds 475 (2009) 446–451.
[24] D.J. Ham, A. Phuruangrat, S. Thongtem, J.S. Lee, Hydrothermal synthesis of monoclinic WO_3 nanoplates and nanorods used as an electrocatalyst for hydrogen evolution reactions from water, Chemical Engineering Journal 165 (2010) 365–369.
[25] I.M. Szilágyi, L. Wang, P.I. Gouma, C. Balázsi, J. Madarász, G. Pokol, Preparation of hexagonal WO_3 from hexagonal ammonium tungsten bronze for sensing NH_3, Materials Research Bulletin 44 (2009) 505–508.
[26] Q. Sun, J. Luo, Z. Xie, J. Wang, X. Su, Synthesis of monodisperse $WO_3 \cdot 2H_2O$ nanospheres by microwave hydrothermal process with L (+) tartaric acid as a protective agent, Materials Letters 62 (2008) 2992–2994.
[27] N. Le Houx, G. Pourroy, F. Camerel, M. Comet, D. Spitzer, WO_3 nanoparticles in the 5–30 nm range by solvothermal synthesis under microwave or resistive heating, The Journal of Physical Chemistry C 114 (2010) 155–161.
[28] J. Sungpanich, T. Thongtem, S. Thongtem, Large-scale synthesis of WO_3 nanoplates by a microwave-hydrothermal method, Ceramics International 38 (2012) 1051–1055.
[29] A. Martínez-de la Cruz, S. Obregón, Synthesis and characterization of nanoparticles of α-$Bi_2Mo_3O_{12}$ prepared by co-precipitation method: Langmuir adsorption parameters and photocatalytic properties with rhodamine B, Solid State Sciences 11 (2009) 829–835.
[30] J.B. Condon, Surface area and porosity determinations by physisorption: measurements and theory, 1st ed., Elsevier, Netherlands, 2006.
[31] Y. Shen, T. Yamazaki, Z. Liu, D. Meng, T. Kikuta, N. Nakatani, Influence of effective surface area on gas sensing properties of WO_3 sputtered thin films, Thin Solid Films 517 (2009) 2069–2072.
[32] Y. Liu, X. Gan, B. Zhou, B. Xiong, J. Li, C. Dong, J. Bai, W. Cai, Photoelectrocatalytic degradation of tetracycline by highly effective TiO_2 nanopore arrays electrode, Journal of Hazardous Materials 171 (2009) 678–683.